January 2013

Solid-Fuel Regression Rate Modeling for Hybrid Rockets

Francesca Favaro
University of California, Irvine

W. Sirignano
University of California, Irvine

M. Manzoni
Politecnico di Milano

L. DeLuca
Politecnico di Milano

Recommended Citation

Francesca Favaro, W. Sirignano, M. Manzoni, and L. DeLuca. "Solid-Fuel Regression Rate Modeling for Hybrid Rockets" *Journal of Propulsion and Power* (2013). https://doi.org/10.2514/1.B34513

Solid Fuel Regression Rate Modeling for Hybrid Rockets

F. M. Favaró and W. A. Sirignano

University of California, Irvine, CA, 92618

M. Manzoni and L. T. DeLuca

Politecnico di Milano, Milan, Italy, 20156

One of the primary parameters in the analysis of the performance of the hybrid rocket engine is the regression rate of the solid fuel. Many studies in the past few years have theoretically claimed, or experimentally shown, a possible dependence between the regression rate itself and the chamber total pressure, but no agreement has been reached about the targeted trend. Such a behavior is generally traced back to the presence of oxygen below the flame zone and of heterogeneous reactions occurring at the surface which affect the pyrolysis law. The experimental program performed for the present work at the Space Propulsion Laboratory of the Politecnico di Milano shows, within the explored operating conditions and the associated uncertainty bands, a neutral trend for the solid fuel regression rate with increasing pressure. The formulation tested was HTPB in Gaseous Oxygen (GOX) at pressures ranging from 4 to 16 bar. A deliberately simplified analytical model which retains the essential physics and accounts for any pressure dependency has been developed, together with the corresponding numerical simulation. We aim to explain pressure dependence and not to reproduce all details of the flow field. The results of this model are presented here. The experimental results are input to the developed model, to give a semi-empirical law for the pyrolysis rate law that could also help to describe a possible pressure dependency.

Nomenclature

B_{TD} = pre-exponential constant [mm/s]

c_p = specific heat [J/(kg K)]

D = port diameter [mm]

E = activation energy [kcal/mol]

$E(T_s)$ = generalized energy per unit mass [J/kg]

f = generic function

G_{ox} = specific oxidizer mass flux [kg/(m^2 s)]

H = energy per unit mass [J/kg]

k = slope of viscosity's linear correlation [m/s]

$\dot{m}$ = constant mass flow [kg/s]

p = pressure [bar]

$\dot{Q}$ = heat flux [W/m^2]

$\dot{r}$ = solid fuel regression rate [mm/s]

R = universal gas constant [kcal/mol]

Re = Reynolds number

t = time [s]

T = temperature [K]

u = horizontal velocity [m/s]

Y = mass fraction

$\boldsymbol{S}$ **= superscalar constant [J/kg]**

Greek Symbols

α = thermal diffusivity [m^2/s]

α_1 = conserved scalar

α_2 = conserved scalar [J/kg]

β = slope of boundary layer's linear correlation

γ = slope of flame position's linear correlation

δ = boundary layer thickness [m]

δ^* = flame position [m]

η = similarity variable

λ = thermal conductivity [W/(m K)]

μ = mixture ratio O/F

ν = kinematic viscosity [m^2/s]

ρ = density [kg/m^3]

Subscripts

$comb$ = combustion

f = fuel

fl = flame

g = gas

ox = oxygen

o = standard condition

pyr = pyrolysis

s = surface

st = stoichiometric

t = turbulent

∞ = free stream

INTRODUCTION

The hybrid rocket is potentially important because it has the promise of combining many of the advantages of both liquid and solid rockets. The simplicity of a solid rocket is in fact merged with the controllability and safety of a liquid one. The hybrid rocket also shows a high degree of flexibility regarding the type of fuel used, and the promise of significant savings in the development and management costs. Unfortunately, though hybrid rocket combustion and propulsion characteristics have been investigated for more than six decades, practical motor development and maturation has not been as actively pursued as that of liquid and solid rocket engines. Classical hybrids suffer from many deficiencies: starting from low regression rates (at least an order of magnitude lower than those of a solid rocket), to poor combustion efficiency (due to the fact that in a hybrid rocket the oxidizer and fuel mixing occurs on a macroscopic scale), through the general difficulty of operating large-scale engines. There is also the possibility of significant longitudinal instabilities during operation, and it is worth considering the fact that in general the mixture ratio will change in time.

A deeper understanding of the phenomena governing the solid fuel regression rate, and the combustion process of the hybrid rocket, could lead to a better comprehension of the reasons determining its performance limits. The classical hybrid-motor combustion model, developed by Marxman and co-workers [1], [2] in the early '60s, is based on turbulent boundary layer transport mechanisms with a diffusion-limited combustion process. Their earlier model did not predict any effect of pressure (or mass fraction of reactive species coming from the oxidizer flow), on the solid fuel regression rate. Actually, the process is considered to be slightly sensitive to the operating conditions, as the macroscopically diffusive flame is controlled by fluid dynamic laws rather than chemical kinetics. The regression of the solid surface is sustained by the thermal energy feedback from the flame, resulting in a purely convective model. Those studies led to the generation of a family of regression rate laws in the form $\dot{r} = f(x)\, G_{ox}^{n}$ with an exponent of about $n \approx 0.8$.

A few years later, in the early '70s, Smoot and Price [3] began to theorize the possibility of a dependence between the solid-fuel regression rate and the operating conditions of the chamber. Their analysis, resulting from intensive experimental studies, showed that the exponent, for the specific oxidizer mass flux G_{ox}, varied not only depending on the value of the same mass flow, but also with changes in the total chamber pressure. Although their early studies showed an enhancement of the regression rate with increasing pressure (assuming a fixed value of the local mass flow),

the authors failed to find a satisfactory theoretical explanation for the results. In a subsequent work [4], the authors conjectured that this cause was to be found in the presence of oxygen at the solid surface. That led to the occurrence of heterogeneous reactions between the solid fuel and the surrounding gaseous oxygen, making the solid interface more reactive. One of the major conclusions was that the assumed dependence on the chamber pressure, increased as the local specific mass flux increased. **However, even though several arguments were proposed in favor of this hypothesis [4], a proved explanation for the witnessed behavior was still missing. One of the rejected explanations regarded the radiative heat flux increase with pressure. For high mass flows, when the thermal radiation is negligible compared to convection, the pressure dependence should be weak. Conversely, for small mass flows, the convective heat transfer should become negligible leading to the independence of the rate of regression on the mass flow and to a considerable change with pressure. Hence, the influence of heat exchanged by radiation would have an opposite effect to that found in the experimental activity and was, therefore, rejected by Smoot and Price. Moreover, in non-metalized fuel grains, such as those considered in this work, at pressures and flux levels of interest for propulsion applications, the heat transferred by convection should be much larger than that transferred by gas-phase radiation or radiation from soot particles in the flow [5]. As a result, the basic characteristics of fuel grain regression may, and will, be explored via an analysis of convective heat transfer in a turbulent boundary layer.**

It is only after the '90s that the inquiry of the dependence on chamber operating conditions was resumed. Two research groups at the University of Delaware and the Pennsylvania State University, have separately conducted some important analysis. The first one, **led by Arisawa and Brill**, has studied in detail the pyrolysis of HTPB [6], [7]. The products resulting from the fuel sublimation were analyzed in different conditions of pressure and heating rate of the polymer. The study shows that, below a certain temperature, the pyrolysis process is governed by the decomposition of the solid matrix (and thus by the rate of formation of gasses from sublimated fuel), while above it the evolution of the gas mixture is controlled by the rate of desorption of gaseous species. They argue that the effect of pressure increase is to lower the transition temperature between the two phenomena. In this sense, seeing the pyrolysis process as a kind of evaporation, the pressure increases to the detriment of the gas desorption from the solid matrix. This is confirmed by the fact that, for higher pressures, the molecules of gas produced are smaller, and the production of monomers is favored over that of oligomers.

The second group, composed primarily by Chiaverini, Kuo and Risha, reports [8] the only evidence in the literature of an actual decrease of the regression rate with pressure. An empirical law that has a strong dependence on the pressure is also fitted:

$$\dot{r} = 3.02\,(Y_{O_2} - 0.21)^{0.19}\,T_{ox}^{1.28}\,\frac{\dot{m}_{ox}^{0.5}}{p^{0.43}} \tag{1}$$

Here Y_{O_2} represents **the freestream oxygen mass fraction**. Another law, in the form of Arrhenius, is also presented and it will be used in the following. The article states that, in the presence of chemically reactive species, the pyrolysis of many polymers is greatly accelerated. The increase in the thermal degradation of the surface in contact with oxygen, is caused by three main factors: the absorption of oxygen by the solid, which changes the structure of the polymer and alters its mechanism of decomposition, exothermic heterogeneous reactions on the surface, and heat transfer due to homogeneous reactions between oxygen and pyrolysis products. The final effect of all of these overlapping processes is not easily predictable.

Although none of the analyzed studies presents a conclusive theoretical explanation of the phenomena at stake, many of the reported data were used for the parameters setting of the following model, and therefore support the development of this research.

EXPERIMENTAL ACTIVITY

The purpose of the testing was to determine whether there is a pressure dependence of the regression rate for nonmetalized hybrid fuel systems. If so, further theoretical studies would help to understand the causes and develop a model of such a behavior. Several tests were conducted at the Space Propulsion Laboratory at Politecnico di Milano, testing HTPB in GOX at increasing pressure values.

To acquire a better understanding of the effects of the operating conditions on the regression rate of the tested fuel, for each test, a fuel sample was placed in a windowed combustor under controlled operating conditions. The combustor was sealed and brought to a selected pressure level using a continuous purge of nitrogen gas. GOX was then introduced into the combustor to burn with the pyrolysis products generated from the fuel sample. The

experimental line is presented in Fig. 1.

The method of ignition used to start the combustion process was an external radiative energy flux from a high-powered CO_2 laser. Around 40 tests were conducted under the following operating conditions:

- Pressure ranged from 4 to 16 bar (58 to 232 psi);
- Oxidizer injection temperature was 298 K;
- Oxidizer mass flow rate (100% GOX) was kept constant at the value of 5 g/s (210 nlpm);
- A cured HTPB fuel formulation was tested.

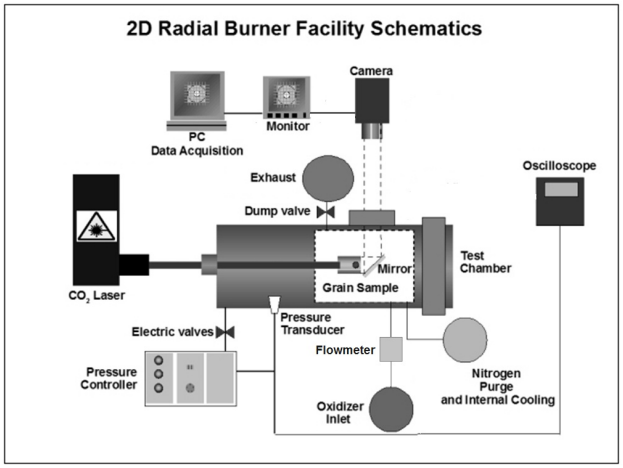

FIG. 1: Schematic view of the experimental line.

Experimental Setup

To operate the test system, three types of control panels were used: one for controlling the oxidizer mass flow, one for the pressurizing system (N_2) connected to a differential manometer and to the electrovalves for the chamber pressure control, and the other for a computerized data acquisition. The signal from the high resolution pressure transducer was monitored and used to adjust the exhaust valve opening to maintain constant the preselected combustor pressure. The data recorded was used to verify that the pressure in the combustor remained nearly constant during the test. The control panels were positioned far enough from the combustor to ensure safe operation.

The combustor was designed with a continuous purge for constant pressure combustion up to 30 bar (441 psi). The feeding mechanism and the head of the combustor are capable of handling cylindrical samples of 20 mm external diameter and length of 30 mm with a circular central port of 4 mm initial diameter. This small burner is contained in a metallic case of about 35 cm in length and 15 cm in diameter. Pictures of the cylindrical sample are reported in Fig. 2.

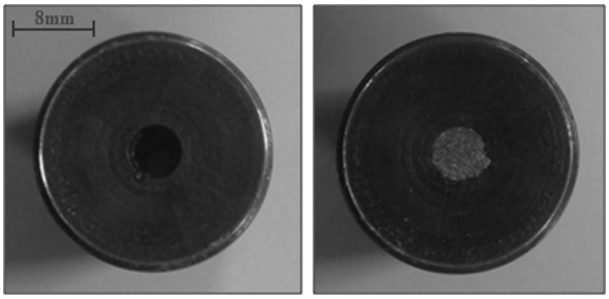

FIG. 2: HTPB cylindrical sample showing central perforation (left) and ignition charge (right).

The combustor case is equipped with two windows ports, one for the camera recording the motion picture of the combustion and one for the laser entrance. The radiant energy flux from the high-powered CO_2 laser was supplied directly to an initiator located at the top of the fuel sample (inside a cylindrical port, also visible in Fig. 2); this method ensures that the ignition of the solid fuel surface is as uniform as possible. A zinc selenide cylinder doped with chromium (ZnSe:Cr) has been used as an infrared transparent window. Two different cameras were used: a `XYBION SVC-09` equipped with a `MOS-485x376` sensor able to collect 25 fps and a `Photron` with `CMOS-1024x1024` sensor able to collect 500 fps. Changes in video frame rate did not affect the regression rate values measured. The videos were instantly compressed and saved on an external hard drive.

Regression Rate Determination

For each value of pressure in the considered range at least 4 trials with their recording were considered. In this way, it is possible to measure the instantaneous variation of the mean port diameter yielding the instantaneous regression rate.

Each video was processed with a frame analysis program. In this case, the RedLake Imaging Motion Scope software `CAMERA` was used. The video was then scrolled frame by frame in order to capture the variation of the port diameter with time. **This was done using a pixel reticle that enabled, for each frame, to capture a suitable number**

of diameters in order to correctly describe the regressing surface. A software package able to detect automatically the regressing surface was also used to analyze the combustion video recordings. In the case of pure HTPB, automatic processing yielded essentially the same results as the manual processing, of course taking much less time while providing much more data. The manual procedure is however expected to be of broader validity since it can be applied also to solid fuels whose regression surface is obscured by a variety of noise sources (observed with high-energy additives), irregularities and anisotropies (observed with wax-based samples), and peculiar phenomena (solid fuel fragmentation) not easily captured by an automatic software.

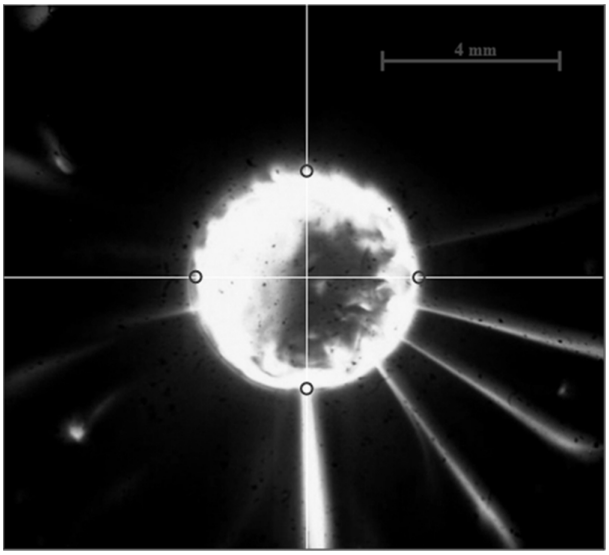

FIG. 3: Frame from a combustion video recording showing the sample burning port. The small circles indicate the regression surface position.

The measure of the port diameter change with time was then converted into millimeters (from the original pixel data) with a calibration of the camera. The history of diameter variation was interpolated in the form

$$D - D_o = f(t) = a \cdot t^n \tag{2}$$

The regression rate is then easily calculated by a simple time differentiation:

$$\dot{r} = \frac{d(D(t)/2)}{dt} = b \cdot t^m \tag{3}$$

so that $b = 0.5\,a \cdot n$ and $m = n - 1$. Knowing the variation of the port diameter, it is possible to deduce also the specific mass flow in time as

$$G_{ox} = \frac{\dot{m}_{ox}}{\pi \frac{D(t)^2}{4}} \equiv \frac{\dot{m}_{ox}}{\pi \frac{(D_o + a \cdot t^n)^2}{4}} \tag{4}$$

from which data are interpolated to find a law in the form

$$\dot{r} = c G_{ox}^q \tag{5}$$

The results obtained for all the trials are reported in Fig. 4 which shows the instantaneous regression rate as a function of the oxidizer mass flux G_{ox}.

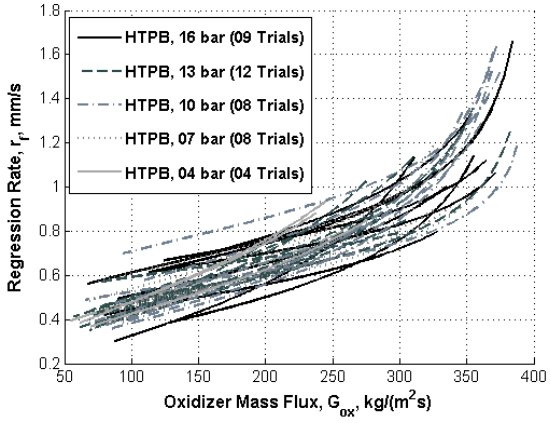

FIG. 4: Comparison of instantaneous regression rate for all the tests showing similar trends for all experimental curves within the explored operating conditions (210 nlpm flow of oxygen was used).

The results shown in Fig. 4 do not highlight a clear trend of the regression rate as a function of pressure. In order to get such an explicit trend of the regression rate as a function of the specific mass flow and pressure, it is necessary to get one single curve for each pressure value. This is done by means of the same interpolation explained before, where the N-curves in the form of Equation 2 (where N is the number of tests), are replaced by one single curve, obtained from the interpolation of all the data coming from different tests at the same pressure. It is then possible to plot the instantaneous regression rate r_f versus the specific oxidizer mass flux G_{ox}. Results are shown in Fig. 5.

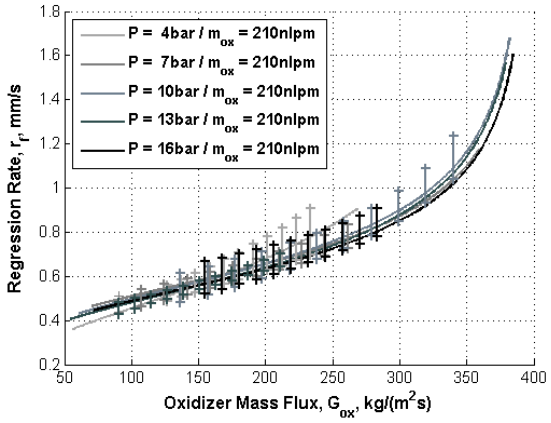

FIG. 5: Instantaneous ensemble regression rate showing negligible pressure dependence within the explored operating conditions.

A significant pressure dependency of the regression rate is not observed. Previous works [9], [10], [11] have established a weak dependence of the regression rate on pressure. In agreement with previous studies [3] other trends are possible. Note that, except for the research at Pennsylvania State University, trials at high pressures ($p \geq 10$ bar) with larger amounts of fuel in the chamber were not found in the literature (or, at least, not testing pure HTPB).

Kuo and co-workers [8] tested HTPB in N_2/O_2 oxidizer (with oxygen mass fraction going from 0.21 to 1) and found that the regression rate increased with free-stream oxygen mass fraction, oxidizer mass flow rate, and oxidizer temperature. However, it decreased with increasing chamber pressure. They collapsed the solid fuel regression rate into a single line using multivariable regression analysis with the power law of Equation (1), where a significant pressure dependence is witnessed. It is not possible to perceive such a clear trend from the results of Fig. 5 of the experimental campaign carried out at the Space Propulsion Laboratory. Two main differences are anyway to be noted: the Penn State experimental campaign used an end burner combustor and, also, the proposed law is computed for laminar conditions.

The following analytical model is intended to be able to account for various observed trends of the regression rate. It should provide a solid base for the development of a new regression rate law that could explain a possible pressure dependency. The goal is to retain the essential physics in the most simplified form. We aim to explain pressure dependence and not to reproduce all details of the flow field. However, given the relevance that a study like the abovementioned [8] carries, the regression rate proposed by

Penn State University will also be tested in the analytical model.

A COMPREHENSIVE ANALYTICAL MODEL

A simplified model for the boundary layer that surrounds the cylindrical solid fuel is presented here. **Given empirical input for a pyrolysis law, it will yield analytical values for the temperature at the surface and at the flame and for the regression rate.** The other unknowns of the model will be the fuel and oxidizer mass fractions, and the flame position. The oxygen will in general be allowed to diffuse below the flame zone, as it is believed to be the major cause for the possible dependence on operating conditions.

Realize that no model can be developed without an empirical representation of one particular process, namely the pyrolysis. We expect the pyrolysis rate might have explicit pressure dependence as well as the temperature and concentration dependences. Furthermore, there can be implicit pressure dependence through the temperature and concentration variables. The analytical representation of the flow and transport physics is required to separate the implicit and explicit dependences on pressure.

Our steady-state model will equate mass burning rates and mass pyrolysis rates with each other and proportion them with the regression rate; mass pyrolysis rate per unit surface area will equal solid-phase density times the surface regression rate. The pyrolysis rate will depend on surface temperature, pressure, and concentrations while those values depend on the behavior of the field, including gas and solid phases. So, determination of the magnitudes of pyrolysis rates, burning rates, and regression rates will depend upon the system constraints. The flame which stands at some distance off the gas-solid interface will be assumed to be diffusion controlled. Transport of mass and energy will be represented analytically, accounting for turbulent mixing in the gas. The pyrolysis-rate law will be determined by matching the theoretical prediction to our experimental results.

Figure 6 shows a schematic of the simplified model that will be used in the following development of the equations for the turbulent-boundary-layer model. The main assumptions are

- the thickness of the turbulent boundary layer (δ) and the transverse position of the flame (δ^*) are considered linearly dependent on x, as commonly in turbulent boundary layer

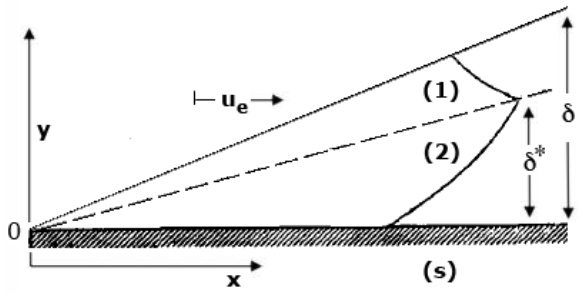

FIG. 6: Schematic representation of the temperature profile in the turbulent boundary layer over the fuel slab.

$$\delta = \delta(x) = \beta x\,; \qquad \delta^* = \delta^*(x) = \gamma x \tag{6}$$

β is an assigned constant (the development of the boundary layer is known), and γ is unknown;

- the solid fuel regression rate is considered uniform in the x direction;
- the diffusion layers in the gas and solid are sufficiently thin compared with the chamber diameter to allow a two-dimensional approximation;
- we consider Pr=Le=Sc=1 in the turbulent condition. This will allow the interchange of α_t, ν_t and D_t, respectively, thermal diffusivity, kinematic viscosity and mass diffusivity;
- the transverse velocity and the streamwise diffusion are neglected;
- low Mach number is assumed;
- all the properties of the fuel (α_f, ρ_f, c_{p_f} and λ_f) will be considered uniform in the solid;
- infinite oxidation kinetic rates are assumed so that a thin flame results with no dissociation of products;
- the turbulent kinematic viscosity is assumed linearly proportional to the x-variable, because turbulent eddy size grows with downstream distance

$$\nu_t = \nu_t(x) \propto kx \tag{7}$$

The variable k may follow different trends, but it is assumed that the ratio u/k remains constant.

Three different domains are considered: two gaseous domains above and below the flame, and a third domain within the solid fuel. For the two gaseous domains, the diffusion equations for mass and energy are written, while in the solid domain, a conduction problem (in y direction) for a semi-infinite slab with the surface in vertical motion at a velocity equal to the regression rate is considered. Given the assumptions described in the three domains, the global problem for oxidizer mass fraction can be stated as

$$u\frac{\partial Y_o}{\partial x} = D_t\frac{\partial^2 Y_o}{\partial y^2}\,; \qquad Y_o(x,\delta) \,=\, Yo_\infty \tag{8}$$

The values at the flame $Y_o(x,\delta^*) \equiv Yo_{fl}$ and at the surface $Y_o(x,0) \equiv Yo_s$ remain to be determined. For the fuel vapor

$$u\frac{\partial Y_f}{\partial x} = D_t\frac{\partial^2 Y_f}{\partial y^2}\,; \qquad Y_f(x,\delta^*) \,=\, 0 \tag{9}$$

where $Y_f(x,0) \equiv Y_{f_s}$ and δ^* remain to be determined and no fuel overreaches the flame zone. For the energy

$$u\frac{\partial T}{\partial x} = \alpha_t\frac{\partial^2 T}{\partial y^2}\,; \qquad T(x,\delta) \,=\, T_\infty \tag{10}$$

here $T(x,\delta^*) \equiv T_{fl}$ and $T(x,0) \equiv T_s$ remain to be determined. Within the solid domain, $y \,\leq\, 0$, the temperature is governed by

$$\frac{\lambda_f}{\rho_f c_p}\frac{d^2T}{dy^2} - \dot{r}\frac{dT}{dy} = 0\,; \qquad T(x,-\infty) \,=\, T_o \tag{11}$$

with the temperature matching T_s at $y \,=\, 0$.

Similar solutions are found in the gas phase with $\eta \,=\,$ y/x. The coordinate transformation causes Equations (8), (9) and (10) to be replaced by ordinary differential equations

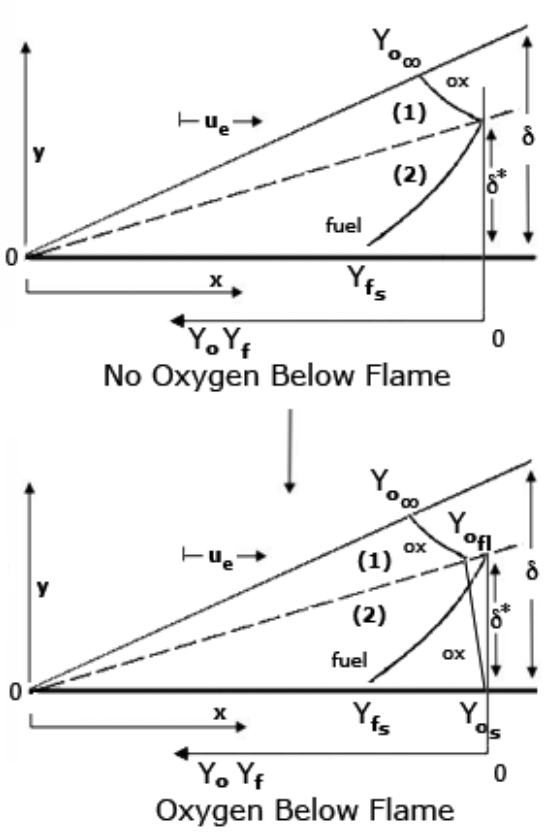

FIG. 7: Schematic representation of the profiles inside the boundary layer.

$$L(Y_o) \equiv \frac{d^2Y_o}{d\eta^2} + \frac{u}{k}\eta\frac{dY_o}{d\eta} = 0 \tag{12}$$

$$L(Y_f) = 0 \tag{13}$$

$$L(T) = 0 \tag{14}$$

with matching conditions at $\eta = 0$ (surface) and $\eta = \gamma$ (flame). The solutions for Domain (1) as shown in Fig. 6 are given by

$$Y_{o_{(1)}} = \frac{(Y_{o_{fl}} - Y_{o_\infty}) \left[\text{erf}\left(\eta\sqrt{\frac{u}{2k}}\right) - \text{erf}\left(\beta\sqrt{\frac{u}{2k}}\right)\right]}{\left[\text{erf}\left(\gamma\sqrt{\frac{u}{2k}}\right) - \text{erf}\left(\beta\sqrt{\frac{u}{2k}}\right)\right]} + Y_{o_\infty} \tag{15}$$

$$\frac{dY_{o_{(1)}}}{d\eta} = \sqrt{\frac{2u_\infty}{k\pi}} \frac{(Y_{o_{fl}} - Y_{o_\infty})}{\left[\text{erf}\left(\gamma\sqrt{\frac{u}{2k}}\right) - \text{erf}\left(\beta\sqrt{\frac{u}{2k}}\right)\right]} e^{-\frac{\eta^2 u_\infty}{2k}} \tag{16}$$

$$Y_{f_{(1)}} = 0 \tag{17}$$

$$\frac{dY_{f_{(1)}}}{d\eta} = 0 \tag{18}$$

$$T_{(1)} = \frac{(T_{fl} - T_\infty) \left[\text{erf}\left(\eta\sqrt{\frac{u}{2k}}\right) - \text{erf}\left(\beta\sqrt{\frac{u}{2k}}\right)\right]}{\left[\text{erf}\left(\gamma\sqrt{\frac{u}{2k}}\right) - \text{erf}\left(\beta\sqrt{\frac{u}{2k}}\right)\right]} + T_\infty \tag{19}$$

$$\frac{dT_{(1)}}{d\eta} = \sqrt{\frac{2u_\infty}{k\pi}} \frac{(T_{fl} - T_\infty)}{\left[\text{erf}\left(\gamma\sqrt{\frac{u}{2k}}\right) - \text{erf}\left(\beta\sqrt{\frac{u}{2k}}\right)\right]} e^{-\frac{\eta^2 u_\infty}{2k}} \tag{20}$$

For Domain (2) of Fig. 6, we obtain

$$Y_{o_{(2)}} = \frac{(Y_{o_{fl}} - Y_{o_s})}{\text{erf}\left(\gamma\sqrt{\frac{u}{2k}}\right)} \text{erf}\left(\eta\sqrt{\frac{u}{2k}}\right) + Y_{o_s} \tag{21}$$

$$\frac{dY_{o_{(2)}}}{d\eta} = \sqrt{\frac{2u_\infty}{k\pi}} \frac{(Y_{o_{fl}} - Y_{o_s})}{\text{erf}\left(\gamma\sqrt{\frac{u}{2k}}\right)} e^{-\frac{\eta^2 u_\infty}{2k}} \tag{22}$$

$$Y_{f_{(2)}} = \frac{-Y_{f_s}}{\text{erf}\left(\gamma\sqrt{\frac{u}{2k}}\right)} \text{erf}\left(\eta\sqrt{\frac{u}{2k}}\right) + Y_{f_s} \tag{23}$$

$$\frac{dY_{f_{(2)}}}{d\eta} = \sqrt{\frac{2u_\infty}{k\pi}} \frac{-Y_{f_s}}{\text{erf}\left(\gamma\sqrt{\frac{u}{2k}}\right)} e^{-\frac{\eta^2 u_\infty}{2k}} \tag{24}$$

$$T_{(2)} = \frac{(T_{fl} - T_s)}{\text{erf}\left(\gamma\sqrt{\frac{u}{2k}}\right)} \text{erf}\left(\eta\sqrt{\frac{u}{2k}}\right) + T_s \tag{25}$$

$$\frac{dT_{(2)}}{d\eta} = \sqrt{\frac{2u_\infty}{k\pi}} \frac{(T_{fl} - T_s)}{\text{erf}\left(\gamma\sqrt{\frac{u}{2k}}\right)} e^{-\frac{\eta^2 u_\infty}{2k}} \tag{26}$$

For the solid fuel domain, the solution is

$$T = T_o + (T_s - T_o)e^{\frac{\dot{r}}{\alpha_f}y} \tag{27}$$

$$\frac{dT}{dy} = \frac{\dot{r}}{\alpha_f}(T_s - T_o)e^{\frac{\dot{r}}{\alpha_f}y} \tag{28}$$

There are seven unknowns of the problem ($\dot{r}$, T_s, T_{fl}, $\delta^* \to \gamma$, Y_{f_s}, Y_{o_s} and $Y_{o_{fl}}$). For the special case where no oxygen is consumed at the surface, $Y_{o_{fl}} = Y_{o_s} = 0$ and only five unknowns are left.

Matching Conditions at Flame and Surface

In general, it is necessary to write seven matching equations between the given profiles, at the flame and at the surface. The resulting algebraic system will be numerically solved, as highly nonlinear. In the following equations, $\dot{m}$ is the mass flow per unit area, μ represents the mixture ratio, and λ is the thermal conductivity in [W/(m K)]. T, Y_o, and Y_f are continuous at the flame although the derivatives are discontinuous. Similarly, T is continuous at the solid interface, while its derivative is discontinuous there.

1. Stoichiometric condition at the flame $y = \delta^*$

$$\frac{\partial Y_{o_{(2)}}}{\partial y} - \frac{\partial Y_{o_{(1)}}}{\partial y} = \mu_{st}\frac{\partial Y_{f_{(2)}}}{\partial y} \tag{29}$$

2. Energy balance at the flame $y = \delta^*$

$$\lambda_{(2)}\frac{\partial T_{(2)}}{\partial y} - \lambda_{(1)}\frac{\partial T_{(1)}}{\partial y} = \dot{Q}_{comb} = -D_t\rho_{fl}\,H_{fl}\frac{\partial Y_{f_{(2)}}}{\partial y} \tag{30}$$

3. Energy balance at the surface $y = 0$

$$\left(\lambda_g\frac{\partial T_{(2)}}{\partial y} - \dot{m}c_{p_g}T_s\right) - \left(\lambda_f\frac{\partial T_{(s)}}{\partial y} - \dot{m}c_{p_f}T_s\right) = -\dot{Q}_{pyr} = -H_{pyr}\rho_f\dot{r} \tag{31}$$

4. Mass balance at the interface $y = 0$

$$\dot{m}_g \equiv \dot{m} = \dot{m}Y_{o_s} + \dot{m}Y_{f_s} - \rho_g D_t \frac{\partial Y_f}{\partial y}_{|_s} - \rho_g D_t \frac{\partial Y_o}{\partial y}_{|_s} = \rho_f \dot{r} \tag{32}$$

5. Stoichiometric condition at the interface $y = 0$.

$$\mu_{pyr}\rho_f \dot{r} = \rho_g D_t \frac{\partial Y_o}{\partial y}_{|_s} - \dot{m}Y_{o_s} \tag{33}$$

Conditions 4 and 5 imply that:

6.

$$-\frac{\mu_{pyr}}{1+\mu_{pyr}} = \frac{\dot{m}_{ox}}{\dot{m}_f} = \frac{-\rho_g D_t \frac{\partial Y_{o_{(2)}}}{\partial y} + \rho_s \dot{r} Y_{o_{(2)}}}{-\rho_g D_t \frac{\partial Y_{f_{(2)}}}{\partial y} + \rho_s \dot{r} Y_{f_{(2)}}} \tag{34}$$

Condition 6 can be applied at the flame location to help determine the unknowns. In order to solve the system, we need one final equation that models the behavior of the pyrolysis rate at the surface:

7. Pyrolysis law at $y = 0$.

As a start, such a law will be modelled with

$$\dot{r} = B_{TD}(1 + cY_{o_s}) \exp\left(-\frac{E_{TD}}{RT_s}\right) \tag{35}$$

Note that for generality Equation (35) is a slightly modified version of the pyrolysis rate law found by the Pennsylvania State University research group in [8]. It contains, inside the pre-exponential factor B_{TD} the experienced pressure dependence, if any. Such a relation, will be replaced in a later section by the semi-empirical law given in Equation (60). Also, note that when no oxygen reaches the surface, condition 5 and 6 are not applicable, Equation (35) assumes the form proposed in [8], and Y_{o_s} and $\frac{\partial Y_o}{\partial y}_{|_s}$ become zero in Equation (32).

Conserved Scalar Approach

We use now the conserved scalars of the problem which will greatly simplify the equations. In fact in this way, it is possible to separate the problem at the flame (in terms of temperature and position) from the other unknowns. To rework the system, it is possible to define two Shvab-Zel'dovich variables [12]:

$$\alpha_1 = Y_o - \mu_{st} Y_f \tag{36}$$

$$\alpha_2 = c_p T + H_{fl} Y_f \tag{37}$$

that satisfy the general problem

$$u \frac{\partial \alpha}{\partial x} = \nu \frac{\partial^2 \alpha}{\partial y^2} \tag{38}$$

where only the boundary conditions at the wall and outside the boundary layer are required, since the two variables are continuous through the flame, being both monotonic. In addition, a linear combination of these variables yields a superscalar (S) [12], which is a constant quantity throughout the domain. Considering, in fact, the derivative of α_1 and α_2 at the surface:

$$\frac{\partial \alpha_1}{\partial y}_{|_s} = \frac{\partial Y_o}{\partial y}_{|_s} - \mu_{st} \frac{\partial Y_f}{\partial y}_{|_s} \tag{39}$$

and

$$\frac{\partial \alpha_2}{\partial y}_{|_s} = c_p \frac{\partial T}{\partial y}_{|_s} + H_{fl} \frac{\partial Y_f}{\partial y}_{|_s} \tag{40}$$

Inserting the given profiles, it is possible to find the following relation

$$\frac{\partial \alpha_2}{\partial y}_{|_s} - \frac{[E(T_s) - H_{fl}\,(1 + \mu_{pyr} - Y_{f_s})]}{(\mu_{pyr} + Y_{o_s}) + \mu_{st}(1 + \mu_{pyr} - Y_{f_s})} \frac{\partial \alpha_1}{\partial y}_{|_s} = 0 \tag{41}$$

where $E(T_s) = c_{p_f}(T_s - T_o) - H_{pyr} + T_s(c_{p_g} - c_{p_f})$ represents the total energy per unit mass of fuel at the surface. Equations (38) and (41) imply that the quantity

$$S = \alpha_2 + \frac{[H_{fl}\,(1 + \mu_{pyr} - Y_{f_s}) - E(T_s)]}{(\mu_{pyr} + Y_{o_s}) + \mu_{st}(1 + \mu_{pyr} - Y_{f_s})} \alpha_1 \tag{42}$$

is a constant. **This quantity will be, from now on, referred to as a superscalar. The superscalar (or supervariable) S is a combination of the primitive dependent variables and becomes uniform over the space. More information regarding the use of superscalars can be found in [12].** Two equations are then given by the equalities $S_{fl} = S_\infty$ and $S_\infty = S_s$, a third one by the pyrolysis law in the Arrhenius form previously presented. Two more equations are derived by comparing the first derivatives of α_1 and α_2 by definition with those derived from the solution of Equation (38). The use of the superscalar at the surface and the flame can replace two of the balance conditions since it was constructed using those conditions. Finally, the mass balance at the wall is considered, while the position of the flame can be calculated from the observation that $\alpha_1(\gamma) \equiv Y_{o_{fl}}$. The final system of seven equations is given by

$$c_p(T_{fl}-T_\infty)+\frac{[H_{fl}\,(1+\mu_{pyr}-Y_{f_s})-E(T_s)]}{(\mu_{pyr}+Y_{o_s})+\mu_{st}(1+\mu_{pyr}-Y_{f_s})}(Y_{o_{fl}}-Y_{o_\infty})=0 \tag{43}$$

$$c_p(T_s-T_\infty)+H_{fl}Y_{f_s}+ + \frac{[H_{fl}\,(1+\mu_{pyr}-Y_{f_s})-E(T_s)]}{(\mu_{pyr}+Y_{o_s})+\mu_{st}(1+\mu_{pyr}-Y_{f_s})}(Y_{o_s}-\mu_{st}Y_{f_s}-Y_{o_\infty})=0 \tag{44}$$

$$\frac{Y_{o_\infty}-Y_{o_s}+\mu_{st}Y_{f_s}}{\mathrm{erf}\left(\beta\sqrt{\frac{u}{2k}}\right)}\sqrt{\frac{2u_\infty}{k_1\pi}}=\frac{\rho_f\dot{r}}{\rho_g k_2}\left[(\mu_{pyr}+Y_{o_s})+\mu_{st}(1+\mu_{pyr}-Y_{f_s})\right] \tag{45}$$

$$\frac{c_p(T_\infty-T_s)-H_{fl}Y_{f_s}}{\mathrm{erf}\left(\beta\sqrt{\frac{u}{2k}}\right)}\sqrt{\frac{2u_\infty}{k_1\pi}}=\frac{\rho_f\dot{r}}{\rho_g k_2}\left[E(T_s)-H_{fl}(1+\mu_{pyr}-Y_{f_s})\right] \tag{46}$$

$$\dot{r}=B_{TD}(1+cY_{o_s})e^{-\frac{E_{TD}}{RT_s}} \tag{47}$$

$$\frac{Y_{o_\infty}-Y_{o_s}+\mu_{st}Y_{f_s}}{\mathrm{erf}\left(\beta\sqrt{\frac{u}{2k}}\right)}\mathrm{erf}\left(\gamma\sqrt{\frac{u}{2k}}\right)+(Y_{o_s}-\mu_{st}Y_{f_s})=Y_{o_{fl}} \tag{48}$$

$$\rho_f\dot{r}=\dot{m}Y_{o_s}+\dot{m}Y_{f_s}+\rho_g k_2\sqrt{\frac{2u_\infty}{k_1\pi}}\left[\frac{Y_{f_s}-(Y_{o_{fl}}-Y_{o_s})}{\mathrm{erf}\left(\gamma\sqrt{\frac{u}{2k}}\right)}\right] \tag{49}$$

where Equations (44) through (47) provide the solution for the problem at the surface in the unknowns T_s, Y_{o_s}, Y_{f_s} and $\dot{r}$, while the other equations are used to solve the problem at the flame, once the solution at the surface has been gained. In the particular case of no oxygen presence in the second gaseous domain, namely $Y_{o_{fl}}=Y_{o_s}=0$, the remaining five unknowns are given by the solution of the following system of Equations (50) to (54)

$$c_pT_{fl}(1-Y_{f_s})=c_pT_s(1-Y_{f_s})+E(T_s)Y_{f_s} \tag{50}$$

$$c_pT_{fl}(1-Y_{f_s})=c_pT_\infty(1-Y_{f_s})+\frac{H_{fl}}{\mu_{st}}Y_{o_\infty}(1-Y_{f_s})-\frac{Y_{o_\infty}}{\mu_{st}}E(T_s) \tag{51}$$

$$\frac{Y_{o_\infty}+\mu_{st}Y_{f_s}}{\mathrm{erf}\left(\beta\sqrt{\frac{u}{2k}}\right)}\sqrt{\frac{2u_\infty}{k\pi}}=\frac{\rho_f\dot{r}}{\rho_g k_2}\mu_{st}(1-Y_{f_s}) \tag{52}$$

$$\dot{r}=B_{TD}e^{-\frac{E_{TD}}{RT_s}} \tag{53}$$

$$\mathrm{erf}\left(\gamma\sqrt{\frac{u}{2k}}\right)=\frac{\mu_{st}Y_{f_s}\mathrm{erf}\left(\beta\sqrt{\frac{u}{2k}}\right)}{Y_{o_\infty}+\mu_{st}Y_{f_s}} \tag{54}$$

where Equation (54) comes from the consideration that $\alpha_1(\gamma)=0$ for this simplified case, and were we now consider

that

$$\frac{\partial Y_o}{\partial y}_{|_s} = 0 \tag{55}$$

in the definition of the first conserved scalar given by Equation (36).

NUMERICAL SIMULATION

The resolution of the system requires a first-guess solution, for the iterative process of error minimization, once the system is written in the form F (x) = 0. Fortunately, it is not necessary to consider all seven unknowns at one time. In fact, it is possible to note that some of the equations have linear behaviors in some of the unknowns. Nevertheless, the solution is particularly sensitive to the first guess. For this reason, the system resolution is accomplished in a "gradual" way, so as to control the correctness of the outputs of the system for more simple cases.

The conserved scalar approach allows the resolution of two separate problems, making the numerical solution process easier. Not only it is possible to consider the flame position as a separate unknown, but it is not necessary to contain it in the non-linear system set of unknowns (usually two or three unknowns, depending whether the presence of oxygen below the flame is considered or not). Considering a constant value of pressure (here 4 bar), and an assigned linear development of the boundary layer (here $\beta = 0.102$ coming from the experimental measure of the Reynolds number $Re \approx 9e^4$) it is possible to obtain the results

$$\boxed{\begin{array}{l} T_s = 789.65 \text{ K}; \quad Y_{f_s} = 0.862; \quad T_{fl} = 2498.4 \text{ K} \\ \dot{r} = 0.383\,\text{mm/s}; \quad \text{erf}(\gamma\sqrt{\frac{u}{2k}}) = 0.5437 \Rightarrow \gamma = 0.0673 \end{array}}$$

using the conserved scalar approach, when no oxygen is considered below the flame. The profiles of the found quantities are shown in dashed lines in Fig. 8. In general, it is expected that when the oxygen presence below the flame is considered, the surface temperature will increase, at the expense of a decrease in the flame temperature. This is caused by the fact that less oxygen is consumed at the flame (resulting in a non-zero value of $Y_{o_{fl}}$), as a part of it diffuses below the flame. When considering oxygen, the following solution is found

$$T_s = 794.99 \text{ K}; \quad Y_{f_s} = 0.861; \quad Y_{o_s} = 0.0035$$

$$\dot{r} = 0.475\,\text{mm/s}; \quad Y_{o_{fl}} = 0.0337; \quad T_{fl} = 2423.6 \text{ K};$$

$$\text{erf}(\gamma\sqrt{\frac{u}{2k}}) = 0.5501 \;\Rightarrow\; \gamma = 0.0683$$

where all the seven unknown variables are considered. These results are shown in solid lines in Fig. 8. The higher value of the regression rate can now be related to several different causes. First, the increase in the surface temperature, as explained before, will enhance the values of the exponential in the Arrhenius form of the pyrolysis law of Equation (35). Also, the value of the pre-exponential constant is different whether an inert local environment is considered or oxygen is present at the surface [8], [13]. The dependence of law (35) on the oxygen mass fraction at the surface gives a small increase of the regression-rate above the value with no oxygen at the solid surface. When considering the presence of oxygen, the flame position is a little higher, as can be seen in Fig. 8.

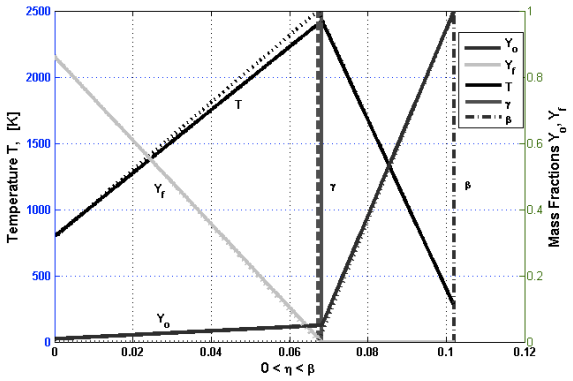

FIG. 8: Comparison of temperature and mass fractions profiles, with and without pressure dependence, obtained with conserved scalar approach: solid lines are obtained when considering the diffusion of oxygen below the flame.

The cause is an augmented value of the transversal fuel mass injection occurring at the surface, as now the incoming oxygen is added to the solid-fuel flux to give the fuel-vapor flux. Having the flame farther from the surface means that the thermal energy feedback from the flame to the surface is smaller, causing the surface temperature to drop. The higher value of T_s is again attributable to the diffusion of oxygen below the flame, as the model is subtracting part of the heat release at the flame, moving it to the surface.

Pressure Dependence

We now consider possible pressure dependences in the system. This can be done by considering two different types of effects: the analytical variation of thermodynamic quantities with pressure and the pressure sensitivity of the pyrolysis rate according to empirical descriptions of spyrolysis rate laws found in the literature.

The first effect is the change of the gas density at the surface ρ_s: inserting the change in the gas density at the surface, through the perfect gas law $\rho_s = \frac{p}{RT_s}$, the regression rate will be increasing with pressure. This is due to an increase in the surface temperature T_s predicted by the model. The temperature rise can in turn be related to the fact that, as the pressure increases, the flame moves toward the surface, enhancing the thermal energy feedback to the solid fuel. The variation with pressure of the kinematic viscosity ν at the wall is also considered. Inside the gaseous domains, this dependence is not taken into account, since it is considered that in the very turbulent regime this value is very slightly variable. At the solid surface, instead, that is treated as a sub-laminar layer, its value is reconnected to the pressure (and temperature) variation through the relation

$$\nu \approx \left[\frac{1}{c_p}(RT)^{3/2}\right]\frac{1}{p} \tag{56}$$

derived from various considerations arising from chemical kinetics and from the fundamental relations of thermodynamics. Interestingly, this quantity is always present, in the equations of the system, multiplied by the density of the gas mixture at the surface. Their product is thus independent of pressure, being the first one directly and the latter inversely proportional to the pressure itself. **Thus, nullifying their effect on each other, the profile of the regression rate is at this point dictated solely by the variation with pressure of the pre-exponential factor B_{TD} in the pyrolysis-rate law.** The global effect of the kinematic viscosity is then to cancel the growth of the regression rate due to the density variation. It will actually bring also a more marked dependence on the temperature that enhances somewhat the value of the regression rate.

The change in the pre-exponential constant of the pyrolysis-rate law is closely related to the regression rate of the solid fuel. The pyrolysis rate is in fact expressed in the system, in both approaches, with a pyrolysis-rate law in the form of Arrhenius ($\dot{r} = B_{TD}\exp\left(-\frac{E_{TD}}{RT_s}\right)$ or $\dot{r} = B_{TD}(1 + cY_{o_s})\exp\left(-\frac{E_{TD}}{RT_s}\right)$, depending whether the presence

of oxygen at the wall is denied or not), as previously presented. **According to the studies conducted at the Pennsylvania State University [8], the pre-exponential factor of this pyrolysis-rate law is to depend on and, more specifically, to decrease with pressure.** From the values given in their work, it is possible to reconstruct a linear law for the variation of this parameter: $B_{TD} = 2.7198 - 0.0634 \cdot p$ where B_{TD} is given in [mm/s] and the pressure in [atm]. Obviously, this pyrolysis-rate law will cause a linear decrease of the regression rate, when no other effects are considered.

Other minor contributions may come from the variation of the molar mass of the gas mixture coming from HTPB pyrolysis, [6], resulting in a variation of the gas constant R for the mixture (that enters in the definition of the kinematic viscosity by law (56), and in the density calculation). Finally, in Reference [14], it is shown how the formulation of HTPB/GOX tends to operate at mixture ratios above the stoichiometric value (about 2.6) when considering an increase in the total pressure in the chamber. The data are quite scarce though, but it would be possible to hypothesize a simple linear pyrolysis-rate law, leading to a lowering of the rate of regression of the solid surface and of performance in general, with departure from the stoichiometric value of the ratio O/F, and lower flame temperature. An analysis of sensitivity to the stoichiometric factor for the oxygen consumption at the surface is also present in the model.

Considering all the effects previously shown, using the law of Equation (35) with a decreasing pre-exponential factor, it is found, as stated before, that the regression rate is actually decreasing with increasing pressure. Figure 9 shows a comparison between the numerical results (and a simple fitting of them in the form $\dot{r} = q\, p^j$) and the trend predicted by Penn State Equation 1. It is possible to see that, even allowing a pressure dependence of the pre-exponential factor, the dependence predicted by Equation 1 is still more marked.

As long as the experienced trend of the solid fuel regression rate is greatly affected by the behavior of the pre-exponential constant B_{TD}, the major concern comes yet from another issue. Even allowing the use of partial experimental results for the setting of the input parameters of the model, we now must address the regression rate dependency on pressure through local effects at the interface. In other words, the Pennsylvania State University group [8], tried to fit the experimental values of $\dot{r}$ with a simple pyrolysis-rate law in the Arrhenius form for first-order reactions. The witnessed trend of $B_{TD}(p)$ is due to the global dependence on pressure of the hybrid combustor. A

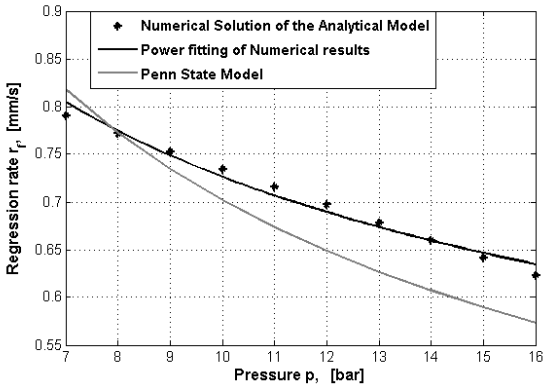

FIG. 9: Numerical results of the regression rate as a function of pressure.

further modification of the pyrolysis-rate law would allow us to address the alleged dependence on pressure through specific local quantities at the surface. The "natural" choice is then to represent the partial density of oxygen in the rate law at the surface; in fact, the whole possibility of a pressure dependency has always been connected to the presence of oxygen below the flame zone. The goal now is to establish a more comprehensive law for the solid fuel pyrolysis rate, that will replace Equation (35) inside the analytical model. We look for a law in the form:

$$\dot{r} = f(\rho_s\, Y_{o_s},\, \rho_s\, Y_{f_s},\, T_s) \tag{57}$$

where f is a fitted function of the oxygen partial density, the fuel partial density and the temperature at the surface. All those quantities will also depend on the values of pressure and of specific mass flux G_{ox}.

COMPARISON WITH EXPERIMENTAL RESULTS AND CONSTRUCTION OF THE SEMI-EMPIRICAL LAW

In order to find the proper function *f*, the experimental results from the Space Propulsion Laboratory will be used. Using the experimental values of the regression rate, the $\dot{r}$ unknown will be removed from the original system of unknowns, and replaced by its experimental values for each pressure. Then, the simulation will be run, and with the found values of T_s, ρ_s and Y_{o_s} it will be possible to fit the new law. However, some modifications in the model need to be applied. Indeed, let us consider the experimental results in terms of instantaneous regression rate, presented before in Fig. 5. We consider that, in these steady-state experiments, both the pyrolysis rate and burning rate are directly proportional to the surface regression rate.

We will analyze pressure values from 7 to 16 bar, as the results for the trials at 4 bar provide solutions only for a rescticted range of G_{ox} values. We now consider G_{ox} to vary from 150 to 300 [kg/(m^2 s)]. For each value of G_{ox} we specify, for the four analyzed values of pressure, the regression rates, as shown in Table I for $G_{ox} = 250$ [kg/(m^2 s)]:

p, bar	Ensemble $\dot{r}$, mm/s	Min. $\dot{r}$, mm/s	Max. $\dot{r}$, mm/s
7	0.748	0.702	0.802
10	0.759	0.703	0.823
13	0.740	0.713	0.791
16	0.726	0.699	0.821

TABLE I: Regression rate variation with pressure. $G_{ox} = 250$ [kg/(m^2 s)].

As said, it is not possible to simply take these values, and use them as an input to the system. In fact, the model has a constant value of the velocity in input (set together with the Reynolds number and the respective boundary layer thickness), while in the experiments, changing the value of pressure (and hence of the density) would imply a different value of the velocity, as we are keeping the value of G_{ox} fixed. Hence, for each cycle the following values must be recalculated:

- the value of the density of the gas ρ;
- the value of the horizontal velocity at the free stream by $u = G_{ox}/\rho$;
- the Reynolds number is actually fixed with G_{ox} as it will depend on the product ρu;
- the value of $\nu_t = k\,x$ in the turbulent domains, as it can be demonstrated that k $\propto \beta^2\,u$. The value of ν_t can be computed by equating two times: the residence time that it would take a particle to get from the leading edge of the slab to an assigned value x, and the time to diffuse from the solid interface to the edge of the boundary layer $\delta = \delta(x)$. See Figure 10.

The solution is then refined with a few effects that were not taken into account in the original model: in fact, it did not reflect a change in the turbulent transport rates due to temperature corrections on the effective Reynolds number when density and viscosity vary through the boundary layer. The representative Reynolds number was calculated using the density and the viscosity at the free stream. As the pressure increases, the surface temperature increases, causing a higher viscosity and a change in density near the surface. Taking averaged values of these quantities (between the free stream and the surface), the Reynolds number for the same velocity, pressure, and length would be lower.

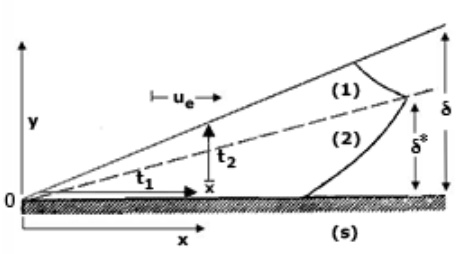

FIG. 10: Times used to compute ν_t.

$$t_1 \doteq t_2, \;\; t_1 = \frac{x}{u}, \;\; t_2 = \frac{\delta^2}{\nu_t} = \frac{\delta^2}{kx}$$

$$\text{as } \delta = \beta x \quad \Rightarrow \quad \frac{x}{u} = \frac{\beta^2 x^2}{kx}$$

$$\text{hence}, \;\; k \propto \beta^2 u$$

This would result in a lower value of the k factor. For this reason, the kinematic viscosity factor k at the free stream (previously set as $k = \beta^2 u_\infty$) will be remodeled as

$$k = \beta^2 u \frac{\rho_s + \rho_\infty}{2\rho_\infty} \tag{58}$$

to account for the density variation through the boundary layer; and the Reynolds number will be calculated using averaged values of density and viscosity

$$Re = \frac{\frac{\rho_s + \rho_\infty}{2} u\, D}{\frac{\mu_s + \mu_\infty}{2}} \tag{59}$$

These corrections bring the results shown in Table II for the value of $G_{ox} = 250$ [kg/(m^2 s)]. This solution, other than the experimental values of $\dot{r}$ taken from the Space Propulsion Laboratory program, does not present any other empiricism.

The new law will consider that the presence of oxygen will increase the pyrolysis rate (and has then a positive sign). The effect of recombination will also be taken into account: as the pressure goes up, we expect an increase in recombination processes. For this reason, an unknown percentage of the partial density of the fuel is subtracted in the new law.

Finally, also the effect of the change in the activation energy from the inert case to the oxidized one is considered in the new law.

p, bar	$\dot{r}$, mm/s	T_s, K	T_{fl}, K	Y_{f_s}	Y_{o_s}
7	0.748	983.8	2448.1	0.7739	3.83e-3
10	0.759	984.3	2488.1	0.7744	1.61e-5
13	0.740	1000.3	2488.3	0.7662	4.31e-5
16	0.726	1014.1	2488.7	0.7592	3.91e-5
p, bar	$Y_{o_{fl}}$	γ	$\rho_s Y_{o_s}$	$\rho_s Y_{f_s}$	ρ_s
7	1.86e-2	0.0840	1.9e-2	3.94	5.10
10	4.83e-3	0.0838	1.2e-4	5.52	7.13
13	4.71e-3	0.0838	3.8e-4	6.84	8.83
16	4.52e-3	0.0838	4.1e-4	8.06	10.61

TABLE II: Example of pressure sensitivity of the different variables after corrections for $G_{ox} = 250$ [kg/(m^2 s)].

The relation will then assume the form, slightly more complicated than Equation (57):

$$\dot{r} = A(c + (\rho_s Y_{o_s})^n) \exp\left(-\frac{E_1}{T_s}\right) - B \exp\left(-\frac{E_2}{T_s}\right) - C(\rho_s Y_{f_s}) \tag{60}$$

where A, c, n, B and C will be fitted using a least squares method for non-linear equations; E_1 and E_2 are in [K], B in [m/s], C in [m^4/(kg s)], n is a number and c and A units are derived from the power of the partial density of oxygen.

The first term is accounting for an increment in the pyrolysis rate, due to the presence of oxygen in the system. The value of E_1 (activation energy divided by the gas constant, here ≈ 1200 K) is set to a value lower than the one for the inert case (here $E_2 \approx 2500$ K), because Pennsylvania State University's experiments [8] (from which the value of E_1 is taken) demonstrate that the presence of oxygen will enhance the pyrolysis (hence a lower activation energy, around a half of the inert one given by Chiaverini and coworkers in [13]). Hence it is, in a sense, like accounting for the oxygen increment twice: once through an increased pre-exponential constant ($c + (\rho_s Y_{o_s})$) and once through a decreased value of E. Considering now a fixed value of $T_s \geq 1000$ K, the first exponential term (with E_1) is around three times bigger than the second term with E_2. The sense of subtracting that value represents a sort of rebalancing of a too-high increase caused by the first term. The contribution of the partial density of oxygen, is presented summed to a constant c. This device is used so that, when considering $Y_{o_s} = 0$ (as in any case in which no oxygen is present in the formulation), the regression rate will not become negative. The last term again is used to account for recombination effects.

Considering a separate fitting for different values of G_{ox}, we see in Fig. 11 that the chosen law of Equation (60) is

suitable to fit the pyrolysis rate in all the cases.

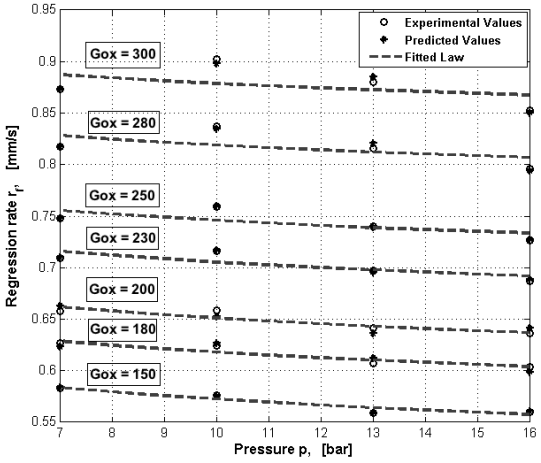

FIG. 11: Fitted law for the pyrolysis rate and experimental values comparing fitted vs. experimental values for the solid fuel regression rate.

We now want to fit the law using all the available data, having hence a single fitting for all the possible values of p and G_{ox}. Combining all the results together in a non-linear system in the form

$$\dot{r} - \left[A(c + (\rho_s Y_{o_s})^n) \exp\left(-\frac{E_1}{T_s}\right) - B \exp\left(-\frac{E_2}{T_s}\right) - C\,(\rho_s Y_{f_s}) \right] = 0 \tag{61}$$

where $\dot{r}$ is now a column vector containing all the experimental results for the different values of G_{ox} and p, with $\rho_s Y_{o_s}$, T_s and $\rho_s Y_{f_s}$ also column vectors, it is possible to get the values for the fitting constants:

$$\begin{aligned} A &= 9.811e-3, \;\; c = 1.562e-2, \;\; n = 2.781e-4 \\ B &= 3.048e-2, \;\; C = 6.314e-7 \end{aligned}$$

Table III shows the percentage error for regression rate at each value of G_{ox} [kg/(m^2 s)], and at the different pressures. The error is always less than the 10%. The highest values of the error are found for low values of the specific mass flow G_{ox}. This means that the model (and the fitting) tends to be more accurate for high values of the Reynolds number, that is to say, for the first instants of functioning of the combustor. Successive instants of time are more poorly approximated.

	$G_{ox} = 150$	$G_{ox} = 180$	$G_{ox} = 200$	$G_{ox} = 230$	$G_{ox} = 250$	$G_{ox} = 280$	$G_{ox} = 300$
$p = 7$	8.307	4.889	6.397	5.186	4.128	1. 766	-0.586
$p = 10$	2.197	2.680	2.966	2.605	1.832	-0.474	-3.147
$p = 13$	-4.301	-2.097	-0.949	-0.047	-0.028	-1.272	-3.242
$p = 16$	-6.971	-5.153	-3.873	-2.711	-2.306	-2.661	-3.851
Aver. Err.	-0.192	0.080	1.135	1.258	0.906	-0.66	-2.706

TABLE III: Percentage error for regression rate at different values of the oxidizer specific mass flux G_{ox} and of pressure p.

CONCLUSION AND FUTURE WORK

A new comprehensive model for the diffusive flame of the hybrid rocket engine was developed. The main difference with respect to the previous models, is that here the possible presence of oxygen below the flame zone is considered. Two different points of view must be taken into account:

1. how the diffusion of oxygen below the flame affects the operating system;

2. how the pressure variation affects the diffusion of oxygen, and hence the regression rate.

Regarding the first point, two effects are experienced. The presence of oxygen at the surface is theoretically responsible for the enhancement of the pyrolysis rate of the solid fuel. This comes from the observation that [8] the presence of oxygen near the fuel surface can enhance the heterogeneous reactions and the overall pyrolysis process, as the surface, in presence of oxygen, will be already reacting with the surrounding oxygen when starting the pyrolysis process. The second effect is instead a more global consideration on the operating conditions in presence of oxygen. From the reported results, it is possible to see that, when the oxygen is allowed to diffuse below the flame zone, a decrease in the flame temperature, together with an increase in the ordinate of the flame position, is witnessed. As was explained, having some oxygen diffuse below the flame, the amount consumed in the combustion is lower, causing a decrease in the flame temperature as more energy is gained at the surface instead. This will affect in a negative way the thermal energy feedback to the surface, yielding a lower surface temperature due to the decreased value of the flame temperature and to the increased distance between the two reacting zones. This effect is however slight, and the net result is still an increase in the regression rate due to the enhancement of the chemical kinetics caused by the presence of oxygen.

The second point investigates how the pressure affects the amount of oxygen that is diffusing below the flame. The research shows that an increase in the total pressure will cause a non-monotonic trend in the behavior of the mass fraction of oxygen both at the surface and at the flame (as can be seen in Table II), causing a consequential non-monotonic behavior of the regression rate. The effects are however slight, and this allows us to deduce that no evident dependence of the regression rate on the chamber total pressure is witnessed under the explored operating conditions.

The following points are then considered achieved by the present work:

- Creation of a model which addresses the variation of pressure for the diffusion flames of the hybrid rocket. Two versions of the model are examined: the first one forcing the mass fraction of oxygen to be null at the wall ($Y_{o_{fl}} \neq 0$ and $Y_{o_s} = 0$) and the second one letting it vary ($Y_{o_{fl}}$, $Y_{o_s} \neq 0$);
- **Development of a semi-empirical law for the pyrolysis rate that will consider its direct dependence on pressure which is determined by clarifying, through the model, the indirect dependence on pressure which is traced through the variation of local quantities at the solid surface, such as temperature and species concentrations.**

Still, the model presents a substantial simplification from both the fluid dynamic, thermodynamic, and chemical perspectives. A refinement of the description of the velocity and temperature fields inside the boundary layer should also reduce the percentage error. Further numerical solutions may be performed starting from the results of this simplified model; more robust and exact simulations can benefit from the use of this first analysis as a guide. Finally, note that the geometry used for the analytical model is a flat slab, while the experiments used a cylindrical sample. The Reynolds number of the analytical model was defined using a characteristic length equal to the initial port diameter. The Reynolds numbers for the first instant of burning in the two geometries equal each other. However, this is not true for the following instants, as the port diameter is changing in time, while the numerical model keeps the characteristic length fixed. Again, further refinement of the model could account for this variation.

ACKNOWLEDGMENTS

The authors wish to thank Mr. C. Paravan, A. Sossi, and E. Duranti for significant help in experimental data handling and reduction. **The authors also wish to thank the anonymous reviewers that helped better expressing some of the ideas contained in this work.**

References

[1] Marxman, G. A., and Wooldridge, C. E., "Fundamentals of Hybrid Boundary Layer Combustion," AIAA Paper 1963-5005.

[2] Gilbert, M., and Marxman, G. A., "Turbulent Boundary Layer Combustion in the Hybrid Rocket," 9^{th} International Symposium on Combustion, 1963, pp. 371-383.

[3] Price, C. F., and Smoot, L. D., "Regression rate mechanisms of nonmetalized hybrid fuel systems," AIAA Paper, 1965-56.

[4] Price, C. F., and Smoot, L. D., "The pressure dependence of hybrid fuel regression rates," AIAA Journal, 1967, Vol. 5 No. 1, pp 102-106.

[5] Sutton, G. P., and Biblarz, O., "Rocket Propulsion Elements." Wiley, New York, Seventh Edition,2001.

[6] Arisawa, H., and Brill, T. B., "Flash pyrolysis of HTPB I: Analysis and implications of the gaseous products," Combustion and Flame, 106:131-143 (1996).

[7] Arisawa, H., and Brill, T. B., "Flash pyrolysis of HTPB II: Implications of the kinetics to combustion of organic polymers," Combustion and Flame, 106:144-154 (1996).

[8] **Risha, G. A., Harting, G. C., Kuo, K. K., Peretz, A., Koch, D. E., Jones, H. S., and Arves, J. P., "Pyrolysis and combustion of solid fuels in various oxidizing environments," AIAA Paper 1998-3184, 34^{th} AIAA/ASME/SAE/ASEE Joint Propulsion Conference and Exhibit, Cleveland, OH, July 13-15, 1998.**

[9] **Smoot, L. D., Price, C. F., and Mihlfeith, C. M., "The pressure dependence of hybrid fuel regression rates," AIAA Paper 1966-113, 3rd Aerospace Sciences Meeting, New York, NY, January 24-26, 1966.**

[10] Altman, D., "Highlights in hybrid rocket propulsion," IWCP In-Space Propulsion, vol. 10, chap. 17, Grafiche GSS, Italy, 2005.

[11] **Karabeyoglu, M. A., Zilliac, G., Cantwell, B. J., De Zilwa, S., and Castelluci, P., "Scale-up tests of high regression rate liquefying hybrid rocket fuels," AIAA Paper 2003-1162, 41^{st} Aerospace Sciences Meeting and Exhibit, Reno, NV, January 6-9, 2003.**

[12] Sirignano, W. A., "A general superscalar for the combustion of liquid fuels," Proceedings of the Combustion Institute,

2002, pp. 535-542.

[13] Chiaverini, M., Harting, G., et al., "Pyrolysis behavior of hybrid rocket solid fuels under rapid heating conditions," AIAA Journal, 1999, Vol. 15 No. 6, pp 888-895.

[14] **Strand, L.D., Jones, M. D., and Ray, R. L., "Characterization of hybrid rocket internal heat flux and HTPB fuel pyrolysis," AIAA Paper 1994-2876, 30th AIAA/ASME/SAE/ASEE Joint Propulsion Conference and Exhibit, Indianapolis, IN, June 27-29, 1994.**

[15] Biblarz, O., and Sutton, G. P., "Rocket Propulsion Elements," Wiley, New York, 7th edition, 2001.

[16] **Evans, B., Boyer, E., Kuo, K., Risha, G., and Chiaverini, M., "Hybrid rocket investigations at Penn State University's high pressure combustion laboratory: Overview and recent results," AIAA Paper 2009-5349, 45th AIAA/ASME/SAE/ASEE Joint Propulsion Conference and Exhibit, Denver, CO, August 2-5, 2009.**

[17] Rabinovitch, B., "Regression rates and the kinetics of polymer degradation," 10th International Symposium on Combustion, 1965, pp. 1395-1404.

[18] Glassman, I., and Yetter, R. A., "Combustion," Academic Press, 4th edition, 2008.

[19] Walter, R. N., "Molar group contributions to heat of combustion," US Department of Transportation - Federal Aviation Admin., DOT-FAA-AR-TN01-75, 2001.

[20] Kubota, N., "Propellants and explosives. Thermochemical Aspects of Combustion," Wiley VCH, 1st edition, 2002.

[21] DeLuca, L. T., "Energetic problems in space propulsion - (orig.) Problemi Energetici in Propulsione Aerospaziale," SPLab, Politecnico di Milano, Preliminary revised edition, 2009.